# Properties of Milky Way globular clusters associated with X-ray sources

Svetoslav Botev[1], Petko Nedialkov[1] & Georgi P. Petrov[1]
Department of Astronomy, Faculty of Physics, Sofia University "St. Kliment Ohridski", Sofia, Bulgaria
botev@phys.uni-sofia.bg

(Submitted on 8 June 2023; Accepted on 13 September 2023)

**Abstract.** The integral X-ray luminosities of 89 Milky Way Globular Clusters within 2 core radii $r_c$ have been estimated using the average X-ray fluxes of individual sources detected in the recent *Chandra*, *XMM-Newton* or *Swift* missions. The X-ray luminosity function is constructed and a limit luminosity $L_X([0.5\text{–}7]\ \mathrm{keV}) = 10^{33.65}\ \mathrm{erg\,s^{-1}}$ is defined, which divides the sample into two groups: 18 high-luminosity clusters and 71 low-luminosity clusters. For both subsamples the Kolmogorov-Smirnov test was applied for the parameters ellipticity, eccentricity of the orbit and estimated number of intermediate mass black holes. The test results show that at a confidence level of 99.9%, the high X-ray luminosity clusters have fewer black holes with intermediate mass than the low X-ray luminosity clusters. In addition, the former have lower ellipticity and higher eccentricity compared to the latter, but at significantly lower confidence levels of 80%.

**Key words:** Globular clusters in the Milky Way, X-ray sources

## Introduction

Globular clusters (GCs) are gravitationally bound aggregations with spheroidal symmetry, that contain tens of thousands to hundreds of thousands of stars. There are $\sim 150$ globular star clusters ( $> 10$ Gyr, Martínez [2019]) in our galaxy (more precisely 157, according to Harris [1996]), which are located at distances between 500 pc and 120 kpc from the center of the Galaxy. A set of dozen GCs parameters, defined by Djorgovski and Meylan, is described in Meylan et al. [1997]. A few years later, Harris [1999] presented the most important characteristics and the main structural parameters of GCs.

Since the first X-ray missions, objects in the Galaxy have been the subject of prime interest. Barnard et al. [2012] pointed out that the first observed objects were predominantly low-mass X-ray binaries (LMXBs) and rarely background galaxies, supernova remnants, or high-mass X-ray binaries (HMXBs). Later on, some researchers like Giesler et al. [2018] throw a light on the circumstance that GCs may include stellar-mass black holes (BHs). The fact that the hard state is typical for BH and neutron star (NS) LMXBs at luminosities of about one tenth of the Eddington luminosity, $L_{Edd}$, is highlighted by Barnard et al. [2014]. For BH XBs a thermally dominated state is typical, which has never been observed in NS XBs (Barnard et al. 2014). As far as Eddington luminosity is concerned, the X-ray bursts of hydrogen-free matter can reach higher luminosities, according to Verbunt et al. [2009], because the Eddington limit is higher in the absence of hydrogen. According to Cheng et al. [2018], by dynamical encounters with encounter rate $\Gamma$ (related to the stellar density $\rho$ and velocity dispersion $\sigma$), hard binaries (with bound energy $|E_b| > E_k$ – average stellar kinetic energy of stars in GCs) transfer their energy to moving stars in close proximity and heat the globular cluster and become harder. However, according to Cheng et al. [2020], by binary-single interactions, soft binaries (with $|E_b| < E_k$) become softer. The rest of the main-sequence (MS) binaries

become more compact, which leads to the formation of many exotic objects in GCs, such as LMXBs, millisecond pulsars (MSPs), cataclysmic variables (CVs), coronal active binaries (ABs) and blue straggler stars (BSS).

The clusters in the Milky Way require individual study because they are scattered (due to the aperture of X-ray telescopes) and because of their proximity to Earth. The observations of Berg et al. [2019] indicate whether a cluster possesses a bright X-ray source and confirm previously proposed correlation between luminous X-ray sources in GCs and dynamical interactions. The accuracy of the X-ray luminosities of these objects is not reliably determinable because they are at different distances from the observer. Here one has to account also that the place of the Solar System within the Milky Way disk prevents us to observe significant number of GCs in our galaxy.

A great number of authors make comparisons between the populations of clusters in M 31 and our galaxy: functions of luminosity, distribution, metallicity, age, etc. In relation to the Milky Way, it is established that there are two types of population, different types of sources, but without bright clusters. For example, Kong et al. [2002] found differences between X-ray GCs in M 31 and X-ray GCs in our galaxy. The luminosity of M 31 X-ray GCs is greater than $L_X = 2 \times 10^{37}$ erg s$^{-1}$ and in the Milky Way there are not similar objects. Furthermore, GCs in M 31 are younger than MW GCs.

The present investigation is motivated by preceding papers of Di Stefano et al. [2002] and Kostov et al. [2005] devoted to M 31 X-ray GCs. In both papers, statistically significant differences in the structural parameters of M 31 GCs containing and missing bright X-ray sources were established.

Based on *Chandra* observations, Di Stefano et al. [2002] constructed X-ray luminosity function of the M 31 and found that systems with $L_X > 10^{37}$ erg s$^{-1}$ are much more frequent in Andoromeda than in the Milky way. Making use of that threshold luminosity, they apply a Kolmogorov-Smirnov (K–S) test to determine if the structural parameters like optical colors and apparent magnitudes, color excesses, metallicities, radial velocities etc., taken from the catalog of Barmby et al. [2002] for populations with and without X-ray sources belong to the same distribution. For example, they proved at the 99% confidence level, that the GCs in M 31 with X-ray sources are optically brighter than the non–X-ray GCs. Di Stefano et al. [2002] were the first to address the structural parameter ellipticity, but due to a poor statistics they failed to distinguish between the populations with and without an X-ray source.

The second attempt was undertaken by Kostov et al. [2005], who studied a representative sample of 110 M 31 GCs due with newly measured X-ray fluxes by the missions *ROSAT, Chandra* and *XMM-Newton*, and with known ellipticity. They found a significant difference in ellipticity (at confidence level of 94%) between a sample of 23 bright X-ray source GC and 87 low X-ray luminosity sources in M 31. Kostov et al. [2005] concluded that the GCs in M 31 with bright X-ray sources are less eccentric than the GCs without X-ray sources.

Although most of the MW GCs have been formed between 12 and 15 Gyr ago, Barmby et al. [2002] suggest that the difference in optical luminosity between the inner and outer GCs in M 31 is due to the circumstance that the brighter GCs are younger (i.e., formed approximately 7–9 Gyr ago) than the fainter ones. That is why GCs located near the center of M 31 evolve

more rapidly than GCs that are situated near the center of the Milky Way. However, the evolution of GCs transforms their cores into smaller and denser ones and this leads to acceleration of the process of formation of X-ray binaries, which leads to more X-ray binaries in M 31 GCs. Crossing time, relaxation time and evolution time $t_{cr} \ll t_{rlx} \ll t_{evol}$ are taken into account in King [1981]. Therefore, these parameters are a basis for construction of theories about the studied globular clusters in our galaxy. Besides, it is well known that the most luminous GCs both in the Milky Way and M 31 are the most spherical ones. When analyzing the results, it is essential to consider the fact that at present we know of $\sim$ 600 GCs in M 31 and $\sim$ 200 GCs in MW.

Such studies have not been provided for the Milky Way clusters and for this reason we have searched for the following globular clusters' parameters in the Galaxy: ellipticity, eccentricity of the orbit and estimated number of black holes with intermediate mass.

Many new parameters have recently become available for a number of GCs, which allows the application of K–S test for them.

In order to differentiate internal from external GCs, along with the age-metallicity relation, the following dynamical parameters are used: apocenter, maximum height from the disc $Z_{max}$ and the orbital circularity parameter $\mathrm{Circ} = L_z/L_z^{circ}$; $L_z$ and $L_z^{circ}$ are, respectively, the Z-component of the angular momentum of a given GC, and the angular momentum of the same GC, moving on a circular orbit with equivalent total energy. The relation $L_z/e$ , where $e$ is eccentricity and $L_z$ is the aforementioned Z-component of the angular momentum of a given GC, divides figuratively the Galaxy's disk and halo fractions.

## 1 Aim of the research

The main goal of this research is a statistical comparison (through the K–S test) of samples of globular clusters from the Milky Way with different integral X-ray luminosities, for which the following parameters are available: X-ray fluxes of individual sources from the missions *Chandra, XMM-Newton* and *Swift*, core radius, distance, extinction E(B–V), ellipticity, eccentricity of the orbit, estimated number of black holes with intermediate mass.

Comparative samples include clusters associated with X-ray sources within $2r_c$ (core radius), with a total X-ray luminosity greater than or less than a prefixed limit of X-ray luminosity.

For this reason, the next sections of the paper are organized as follows. Section 2 represents K–S test and its usage for a quantitative assessment of the statistical distinguishability of two samples – in our case, consisting of X-ray globular cluster sources with previously calculated different luminosities. In Section 3, we describe extracted data from the data sources – the catalogs, connected with recent large X-ray missions (see the first paragraph of this section) and pay attention to the processing data within $2r_c$ range. Section 4 reports our analysis, based on chosen structural parameters and compares them in a brief way. Afterwards we discuss shortly the observational results by means of discussing figures, presenting data correlations, and expressing a set of constrained data in an orderly constructed relative table. Then we explore the significance of our results for future investigations, concerning GCs in the Galaxy. Finally, we summarize our conclusions.

## 2 Statistical K–S test

In order to make a quantitative assessment of the statistical distinguishability of two samples, the K–S test has been applied. Its immediate application is appropriate for unbound distributions (cumulative probability) that are a function of one independent variable. The test calculates two quantities -– the so-called D-statistics (D-stat.) as well as the K–S confidence level, in order to reject the null hypothesis, according to which both distributions in principle are derived from one and the same parental distribution (i.e. they are statistically indistinguishable). The rejection of the null hypothesis corresponds to large values of confidence level, which means that small values of confidence level indicate statistical indistinguishability of the two samples.

## 3 Observational data

### 3.1 Data sources

The catalog of Harris [1996] is used as a reference source for GCs in the Galaxy and their ellipticities $\eta$ . It contains detailed data for 157 clusters. This list can be supplemented by another 57 clusters, discovered after 2005 (see Ryu et al. [2018]), for which, however, accurate and homogenized morphological data are not available. A significant number of clusters (∼30), located behind the bulge and close to the plane of the disc, are not detected yet.

Data on the X-ray fluxes of individual sources in the GCs are taken from recent catalogs of large X-ray missions, available through the Vizier Internet platform of the Astronomical Data Center in Strasbourg, France. These include: The *Chandra* Source Catalog (CSC), Release 2.0 (Evans et al. 2010-2019), *XMM-Newton* Serendipitous Source Catalog 4XMM-DR9 (Webb et al. 2020) and 2SXPS *Swift* X-ray telescope point source catalog (Evans et al. 2020).

In the present research, all sources were initially selected within the visible outlines of each globular cluster (that is up to distances at which the stellar density of the stars in the cluster decreases approximately to the background stellar density). Subsequently, in order to avoid bright background X-ray sources and following the result of Verbunt [2001] that the brightest sources were observed in the innermost areas of the clusters, in this research, the sources have been limited to within 2 core radii $r_c$ in order to account for the integrated flux of the respective cluster.

Fig. 1 represents *Chandra* fluxes $F_{\rm X}$[0.5–7] keV of individual X-ray sources in the vicinity of NGC 6440 globular cluster (in logarithmic scale on the ordinate axis) as a function of their distance from the cluster center (see the ratio $\rm r/r_c$ on the abscissa axis), as well as their space distribution superimposed in the view plane (see the upper right corner) on a 6×6 arcmin$^2$ optical image of the cluster from the *Digitized Sky Survey*[1]. Generally, it illustrates the principle of selection by means of the radial distribution of the fluxes (and luminosities, as far as the sources are at the same distance from the observer)

[1] https://archive.stsci.edu/dss/

of the individual X-ray sources in the globular cluster NGC 6440 within 8 nuclear radii (about 1.12 arcmin on the sky).

Table 1 compiles the available data needed to calculate the X-ray luminosities $L_X$ for some of the 147 Milky Way GCs from the Harris [1996] catalog. In this table are listed: heliocentric distance $R_{Sun}$, color excess E(B–V), core radius $r_c$, farmost distance of the individual X-ray source within 2 core radii from the globular cluster center $r_{max}$ (if denoted with !, then it is the distance of the individual X-ray source closest to the globular cluster center), $n_x$ – total number of registered individual X-ray sources within 2 core radii, summed X-ray flux $F_{\rm X}([0.5-7]$ keV) of all considered individual sources. The last column indicates the mission of the finally adopted fluxes C – for *Chandra*, S – for *Swift*, N – for *XMM-Newton* mission or AVE – for the average of two missions. Note that there are clusters with available X-ray data but without any sources detected within 2 core radii. The latter will be designated as low central X-ray luminosity (low $L_X$) clusters (see Table 2). However, their ellipticity, total number of black holes with intermediate mass and orbital eccentricity can be used in K–S tests, always including them in the samples with X-ray luminosity lower than a certain threshold luminosity.

### 3.2 Processing data

The most numerous data on X-ray fluxes are included in the catalog of Evans et al. [2010-2019] from the mission *Chandra* in the range of photon energies 0.5 – 7 keV, with efficient energy of the order of 2.3 keV. For this reason, data for other fluxes has been converted to this range using the following relations:

*Chandra* $\rightarrow$ *Chandra*:
$F_{\rm X}([0.5-7]\ {\rm keV}) = (6.5/9.9)F_{\rm X}([0.1-10]\ {\rm keV})\,;$

*XMMN* $\rightarrow$ *Chandra*:
$F_{\rm X}([0.5-7]\ {\rm keV}) = F_{\rm X}([0.5-1]\ {\rm keV}) + F_{\rm X}([1-2]\ {\rm keV}) +$
$+F_{\rm X}([2-4.5\ {\rm keV}) + F_{\rm X}([4.5-10]\ {\rm keV})/3\,;$

*Swift* $\rightarrow$ *Chandra*:
$F_{\rm X}([0.5-7]\ {\rm keV}) = (6.5/9.7)F_{\rm X}([0.3-10]\ {\rm keV})\,.$

There are 24 clusters with 2 independent estimates from different X-ray missions. The difference of the *XMMN* X-ray total flux minus *Chandra* X-ray total flux of 24 Milky Way GCs in the range [0.5–7] keV (on the ordinate axis) as a function of *Chandra* X-ray total flux (on the abscissa axis) is given in logarithmic scale in Fig. 2, where both fluxes are summed within 2 core radii. In general, for 20 of the GCs the agreement is around or less than one order of magnitude. For them the averaged fluxes were adopted. Note that the flux amplitude reflects the X-ray variability of a certain source with time rather than the much lower error of the globular cluster total flux on a fixed time epoch.

For three outliers on Fig. 2, namely GCs Terzan 5, NGC 2808 and NGC 6626, however, we adopted the larger flux values without averaging, assuming that their high state represents their X-ray luminosity. For 8 clusters there are no individual sources within $2r_c$ and, therefore, they are assigned to the

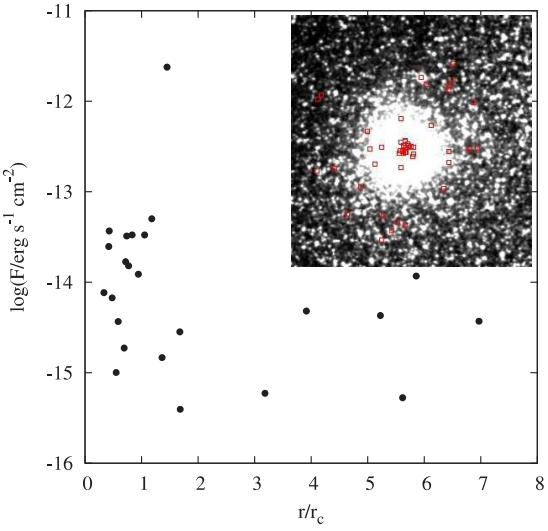


**Fig. 1.** *Chandra* fluxes $F_{\rm X}$([0.5–7] keV) of individual X-ray sources (filled circles) in the vicinity of NGC 6440 globular cluster as a function of their distance from the cluster center. Their space distribution (open squares) in the view plane is superimposed (upper right corner) on a 6×6 arcmin$^2$ optical image of the cluster from *Digitized Sky Survey*.

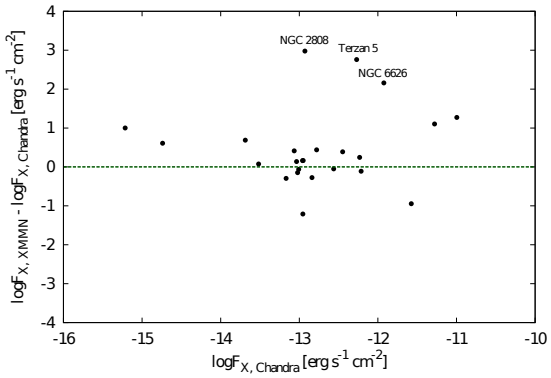


**Fig. 2.** *XMMN* X-ray total flux minus *Chandra* X-ray total flux of 24 Milky Way GCs in the range [0.5–7] keV as a function of *Chandra* X-ray total flux. Both fluxes are summed within 2 core radii.

clusters with low X-ray luminosity (they are denoted as low $L_X$ in Table 2, which means zero flux in the area of $2r_c$). Finally, numerical estimates of the total X-ray fluxes in the range of [0.5–7] keV within $2r_c$ for 89 GCs are available (see Table 2).

**Table 1.** Data for Milky Way GCs, used to estimate their X-ray luminosities $L_X$: heliocentric distance $R_{Sun}$, color excess E(B–V), core radius $r_c$, farmost distance of the individual X-ray source within 2 core radii from the globular cluster center $r_{max}$ (if denoted with !, then it is the distance of the individual X-ray source closest to the globular cluster center), $n_x$ – total number of registered individual X-ray sources within 2 core radii, summed X-ray flux $F_{\rm X}([0.5-7]$ keV) of all considered individual sources. The last column indicates the mission of the finally adopted fluxes C – for *Chandra*, S - for *Swift*, N - for *XMM-Newton* mission or AVE - for the average of two missions.

| ID | $R_{Sun}$ | E(B–V) | $r_c$ | $r_{max}$ | $n_x$ | $F_{\rm X}([0.5-7]$ keV) Ch./Sw. | $r_{max}$ | $n_x$ | $F_{\rm X}([0.5-7]$ keV) XMMN | Adopted $F_{\rm X}([0.5-7]$ keV) | Mission |
|---|---|---|---|---|---|---|---|---|---|---|---|
| | kpc | mag | arcmin | arcmin | | mW/m$^2$ | arcmin | | mW/m$^2$ | mW/m$^2$ | |
| (1) | (2) | (3) | (4) | (5) | (6) | (7) | (8) | (9) | (10) | (11) | (12) |
| NGC 104 | 4.5 | 0.04 | 0.36 | 0.720 | 155 | 0.141e–11 | – | – | – | 0.141e–11 | C |
| NGC 288 | 8.9 | 0.03 | 1.35 | 2.372 | 9 | 0.615e–13 | – | – | – | 0.615e–13 | C |
| NGC 362 | 8.6 | 0.05 | 0.18 | 0.306 | 18 | 0.927e–13 | – | – | – | 0.927e–13 | C |
| Whiting 1 | 30.1 | 0.03 | 0.25 | – | – | – | – | – | – | – | – |
| NGC 1261 | 16.3 | 0.01 | 0.35 | 0.209 | 1 | 1.648e–14 | – | – | – | 1.648e–14 | C |
| Pal 1 | 11.1 | 0.15 | 0.01 | – | – | – | – | – | – | – | – |
| AM 1 | 123.3 | 0.00 | 0.17 | – | – | – | – | – | – | – | – |
| Eridanus | 90.1 | 0.02 | 0.25 | – | – | – | – | – | – | – | – |
| Pal 2 | 27.2 | 1.24 | 0.17 | 0.596! | 1 | 1.827e–13 | – | – | – | zero flux | C |
| NGC 1851 | 12.1 | 0.02 | 0.09 | 0.170 | 7 | 0.526e–11 | 0.170 | 1 | 6.693e–11 | 0.361e–10 | AVE |
| NGC 1904 | 12.9 | 0.01 | 0.16 | 0.204 | 4 | 0.455e–13 | – | – | – | 0.455e–13 | C |
| NGC 2298 | 10.8 | 0.14 | 0.31 | 1.741 | 1 | 5.900e–14 | – | – | – | 5.900e–14 | S |
| NGC 2419 | 82.6 | 0.08 | 0.32 | – | – | – | – | – | – | – | – |
| Ko 2 | 34.7 | 0.08 | 0.25 | – | – | – | – | – | – | – | – |
| Pyxis | 39.4 | 0.21 | – | – | – | – | – | – | – | – | – |
| NGC 2808 | 9.6 | 0.22 | 0.25 | 0.388 | (11) | (0.118e–12) | 0.318 | 3 | 0.112e–09 | 0.112e–09 | N |
| E 3 | 8.1 | 0.30 | 1.87 | 1.964 | 3 | 0.172e–13 | – | – | – | 0.172e–13 | C |
| Pal 3 | 92.5 | 0.04 | 0.41 | – | – | – | – | – | – | – | – |
| NGC 3201 | 4.9 | 0.24 | 1.30 | 2.375 | 17 | 0.680e–13 | 2.378 | 5 | 0.345e–13 | 0.512e–13 | AVE |
| Pal 4 | 108.7 | 0.01 | 0.33 | – | – | – | – | – | – | – | – |
| Ko 1 | 48.3 | 0.01 | 0.33 | – | – | – | – | – | – | – | – |
| NGC 4147 | 19.3 | 0.02 | 0.09 | – | – | – | – | – | – | – | – |
| NGC 4372 | 5.8 | 0.39 | 1.75 | 3.111 | 2 | 1.601e–13 | – | – | – | 1.601e–13 | N |
| Rup 106 | 21.2 | 0.20 | 1.00 | – | – | – | – | – | – | – | – |
| NGC 4590 | 10.3 | 0.05 | 0.58 | 0.893 | 2 | 4.690e–14 | – | – | – | 4.690e–14 | S |
| NGC 4833 | 6.6 | 0.32 | 1.00 | – | – | – | – | – | – | – | – |
| NGC 5024 | 17.9 | 0.02 | 0.35 | 0.716 | 3 | 0.281e–13 | – | – | – | 0.281e–13 | C |
| NGC 5053 | 17.4 | 0.01 | 2.08 | – | – | – | – | – | – | – | – |

**Table 1.** (continued)

| ID | $R_{Sun}$ | E(B–V) | $r_c$ | $r_{max}$ | $n_x$ | $F_{\rm X}([0.5-7]$ keV) Ch./Sw. | $r_{max}$ | $n_x$ | $F_{\rm X}([0.5-7]$ keV) XMMN | Adopted $F_{\rm X}([0.5-7]$ keV) | Mission |
|---|---|---|---|---|---|---|---|---|---|---|---|
| | kpc | mag | arcmin | arcmin | | mW/m$^2$ | arcmin | | mW/m$^2$ | mW/m$^2$ | |
| (1) | (2) | (3) | (4) | (5) | (6) | (7) | (8) | (9) | (10) | (11) | (12) |
| NGC 5139 | 5.2 | 0.12 | 2.37 | 4.715 | 121 | 0.612e–12 | 4.651 | 31 | 0.476e–12 | 0.544e–12 | AVE |
| NGC 5272 | 10.2 | 0.01 | 0.37 | 0.716 | 6 | 0.477e–12 | – | – | – | 0.477e–12 | C |
| NGC 5286 | 11.7 | 0.24 | 0.28 | 0.569 | 4 | 0.330e–13 | – | – | – | 0.330e–13 | C |
| AM 4 | 32.2 | 0.05 | 0.41 | – | – | – | – | – | – | – | – |
| NGC 5466 | 16.0 | 0.00 | 1.43 | – | – | – | 9.256! | 1 | 3.414e–15 | zero flux | N |
| NGC 5634 | 25.2 | 0.05 | 0.09 | – | – | – | – | – | – | – | – |
| NGC 5694 | 35.0 | 0.09 | 0.06 | – | – | – | – | – | – | – | – |
| IC 4499 | 18.8 | 0.23 | 0.84 | – | – | – | – | – | – | – | – |
| NGC 5824 | 32.1 | 0.13 | 0.06 | 0.753! | 1 | 5.346e–15 | – | – | – | zero flux | C |
| Pal 5 | 23.2 | 0.03 | 2.29 | 4.700 | 6 | 0.138e–12 | – | – | – | 0.138e–12 | C |
| NGC 5897 | 12.5 | 0.09 | 1.40 | – | – | – | – | – | – | – | – |
| NGC 5904 | 7.5 | 0.03 | 0.44 | 0.716 | 10 | 0.503e–13 | – | – | – | 0.503e–13 | C |
| NGC 5927 | 7.7 | 0.45 | 0.42 | 0.773 | 10 | 0.147e–13 | – | – | – | 0.147e–13 | C |
| NGC 5946 | 10.6 | 0.54 | 0.08 | 0.123 | 1 | 6.091e–16 | 0.042 | 1 | 6.110e–15 | 0.336e–14 | AVE |
| BH 176 | 18.9 | 0.54 | 0.90 | – | – | – | – | – | – | – | – |
| NGC 5986 | 10.4 | 0.28 | 0.47 | – | – | – | – | – | – | – | – |
| Lynga 7 | 8.0 | 0.73 | 0.90 | – | – | – | – | – | – | – | – |
| Pal 14 | 76.5 | 0.04 | 0.82 | – | – | – | – | – | – | – | – |
| NGC 6093 | 10.0 | 0.18 | 0.15 | 0.302 | 11 | 0.143e–12 | – | – | – | 0.143e–12 | C |
| NGC 6121 | 2.2 | 0.35 | 1.16 | 2.332 | 48 | 0.256e–12 | – | – | – | 0.256e–12 | C |
| NGC 6101 | 15.4 | 0.05 | 0.97 | 1.132 | 1 | 3.696e–14 | – | – | – | 3.696e–14 | S |
| NGC 6144 | 8.9 | 0.36 | 0.94 | 1.909 | 9 | 0.939e–13 | – | – | – | 0.939e–13 | C |
| NGC 6139 | 10.1 | 0.75 | 0.15 | 0.195 | 7 | 0.883e–13 | – | – | – | 0.883e–13 | C |
| Terzan 3 | 8.2 | 0.73 | 1.18 | 1.937 | 10 | 0.257e–13 | – | – | – | 0.257e–13 | C |
| NGC 6171 | 6.4 | 0.33 | 0.56 | 1.106 | 1 | 4.455e–14 | – | – | – | 4.455e–14 | S |
| 1636-283 | 8.3 | 0.46 | 0.50 | – | – | – | – | – | – | – | – |
| NGC 6205 | 7.1 | 0.02 | 0.62 | 1.150 | 12 | 0.112e–12 | 1.106 | 8 | 0.164e–12 | 0.138e–12 | AVE |
| NGC 6229 | 30.5 | 0.01 | 0.12 | – | – | – | – | – | – | – | – |
| NGC 6218 | 4.8 | 0.19 | 0.79 | 1.472 | 4 | 0.927e–13 | – | – | – | 0.927e–13 | C |
| FSR 1735 | 9.8 | 1.42 | 0.39 | – | – | – | – | – | – | – | – |
| NGC 6235 | 11.5 | 0.31 | 0.33 | – | – | – | – | – | – | – | – |
| NGC 6254 | 4.4 | 0.28 | 0.77 | – | – | – | – | | – | – | – |
| NGC 6256 | 10.3 | 1.09 | 0.02 | 0.038 | 1 | 8.160e–14 | – | | – | 8.160e–14 | C |

**Table 1.** (continued)

| ID | $R_{Sun}$ | E(B–V) | $r_c$ | $r_{max}$ | $n_x$ | $F_X$([0.5− 7] keV) Ch./Sw. | $r_{max}$ | $n_x$ | $F_X$([0.5− 7] keV) XMMN | Adopted $F_X$([0.5− 7] keV) | Mission |
|---|---|---|---|---|---|---|---|---|---|---|---|
| | kpc | mag | arcmin | arcmin | | mW/m$^2$ | arcmin | | mW/m$^2$ | mW/m$^2$ | |
| (1) | (2) | (3) | (4) | (5) | (6) | (7) | (8) | (9) | (10) | (11) | (12) |
| Pal 15 | 45.1 | 0.40 | 1.20 | – | – | – | – | | – | – | – |
| NGC 6266 | 6.8 | 0.47 | 0.22 | 0.394 | 27 | 0.586e–12 | 0.381 | 2 | 0.103e–11 | 0.808e–12 | AVE |
| NGC 6273 | 8.8 | 0.38 | 0.43 | 0.556 | 1 | 5.454e–14 | – | – | – | 5.454e–14 | S |
| NGC 6284 | 15.3 | 0.28 | 0.07 | – | – | – | – | – | – | – | – |
| NGC 6287 | 9.4 | 0.60 | 0.29 | 0.506 | 4 | 0.489e–13 | – | – | – | 0.489e–13 | C |
| NGC 6293 | 9.5 | 0.36 | 0.05 | 0.040 | 1 | 1.618e–14 | – | – | – | 1.618e–14 | C |
| NGC 6304 | 5.9 | 0.54 | 0.21 | 0.340 | 15 | 0.983e–13 | 0.381 | 1 | 8.546e–14 | 0.919e–13 | AVE |
| NGC 6316 | 10.4 | 0.54 | 0.17 | – | – | – | – | – | – | – | – |
| NGC 6341 | 8.3 | 0.02 | 0.26 | 0.437 | 8 | 0.519e–13 | – | – | – | 0.519e–13 | C |
| NGC 6325 | 7.8 | 0.91 | 0.03 | 0.082 | 2 | 0.891e–14 | – | – | – | 0.891e–14 | C |
| NGC 6333 | 7.9 | 0.38 | 0.45 | 0.515 | 2 | 0.137e–13 | – | – | – | 0.137e–13 | C |
| NGC 6342 | 8.5 | 0.46 | 0.05 | 0.114 | 1 | 1.624e–15 | – | – | – | 1.624e–15 | C |
| NGC 6356 | 15.1 | 0.28 | 0.24 | – | – | – | – | – | – | – | – |
| NGC 6355 | 9.2 | 0.77 | 0.05 | 0.098 | 2 | 0.655e–14 | – | – | – | 0.655e–14 | C |
| NGC 6352 | 5.6 | 0.22 | 0.83 | – | – | – | – | – | – | – | – |
| IC 1257 | 25.0 | 0.73 | 0.25 | – | – | – | – | – | – | – | – |
| Terzan 2 | 7.5 | 1.87 | 0.03 | 0.022 | 1 | 2.330e–11 | – | – | – | 2.330e–11 | C |
| NGC 6366 | 3.5 | 0.71 | 2.17 | 3.911 | 10 | 0.923e–13 | 4.207 | 6 | 0.127e–12 | 0.110e–12 | AVE |
| Terzan 4 | 7.2 | 2.00 | 0.90 | – | – | – | 8.140! | 1 | 3.486e–13 | zero flux | N |
| HP 1 | 8.2 | 1.12 | 0.03 | – | – | – | – | – | – | – | – |
| NGC 6362 | 7.6 | 0.09 | 1.13 | 2.251 | 13 | 0.472e–13 | – | – | – | 0.472e–13 | C |
| Liller 1 | 8.2 | 3.07 | 0.06 | 0.020 | 1 | 2.489e–11 | – | – | – | 2.489e–11 | C |
| NGC 6380 | 10.9 | 1.17 | 0.34 | – | – | – | – | – | – | – | – |
| Terzan 1 | 6.7 | 1.99 | 0.04 | 0.639! | 1 | 1.408e–14 | – | – | – | zero flux | C |
| Ton 2 | 8.2 | 1.24 | 0.54 | – | – | – | – | – | – | – | – |
| NGC 6388 | 9.9 | 0.37 | 0.12 | 0.238 | 22 | 0.356e–12 | 0.016 | 1 | 8.701e–13 | 0.613e–12 | AVE |
| NGC 6402 | 9.3 | 0.60 | 0.79 | – | – | – | – | – | – | – | – |
| NGC 6401 | 10.6 | 0.72 | 0.25 | 0.339 | 4 | 0.414e–13 | – | – | – | 0.414e–13 | C |
| NGC 6397 | 2.3 | 0.18 | 0.05 | 0.108 | 4 | 0.625e–12 | – | – | – | 0.625e–12 | C |
| Pal 6 | 5.8 | 1.46 | 0.66 | – | – | – | – | – | – | – | – |
| NGC 6426 | 20.6 | 0.36 | 0.26 | – | – | – | – | – | – | – | – |
| Djorg 1 | 13.7 | 1.58 | 0.50 | – | – | – | – | – | – | – | – |
| Terzan 5 | 6.9 | 2.28 | 0.16 | 0.318 | (34) | (0.536e–12) | 0.246 | 2 | 0.308e–09 | 0.308e–09 | N |

**Table 1.** (continued)

| ID | $R_{Sun}$ | E(B–V) | $r_c$ | $r_{max}$ | $n_x$ | $F_X$([0.5− 7] keV) Ch./Sw. | $r_{max}$ | $n_x$ | $F_X$([0.5− 7] keV) XMMN | Adopted $F_X$([0.5− 7] keV) | Mission |
|---|---|---|---|---|---|---|---|---|---|---|---|
| | kpc | mag | arcmin | arcmin | | mW/m$^2$ | arcmin | | mW/m$^2$ | mW/m$^2$ | |
| (1) | (2) | (3) | (4) | (5) | (6) | (7) | (8) | (9) | (10) | (11) | (12) |
| NGC 6440 | 8.5 | 1.07 | 0.14 | 0.235 | 18 | 0.266e–11 | 0.043 | 1 | 3.028e–13 | 0.148e–11 | AVE |
| NGC 6441 | 11.6 | 0.47 | 0.13 | 0.237 | 9 | 0.101e–10 | 0.083 | 1 | 1.887e–10 | 0.994e–10 | AVE |
| Terzan 6 | 6.8 | 2.35 | 0.05 | 0.103 | 1 | 1.250e–11 | – | – | – | 1.250e–11 | C |
| NGC 6453 | 11.6 | 0.64 | 0.05 | 0.053 | 2 | 0.153e–12 | – | – | – | 0.153e–12 | C |
| UKS 1 | 7.8 | 3.14 | 0.15 | – | – | – | – | – | – | – | – |
| NGC 6496 | 11.3 | 0.15 | 0.95 | – | – | – | – | – | – | – | – |
| Terzan 9 | 7.1 | 1.76 | 0.03 | 0.064 | 1 | 9.448e–14 | – | – | – | 9.448e–14 | C |
| Djorg 2 | 6.3 | 0.94 | 0.33 | 0.312 | 1 | 3.907e–13 | – | – | – | 3.907e–13 | S |
| NGC 6517 | 10.6 | 1.08 | 0.06 | 0.052 | 1 | 8.778e–15 | – | – | – | 8.778e–15 | C |
| Terzan 10 | 5.8 | 2.40 | 0.90 | – | – | – | – | – | – | – | – |
| NGC 6522 | 7.7 | 0.48 | 0.05 | 0.266 | 1 | 4.177e–14 | – | – | – | 4.177e–14 | C |
| NGC 6535 | 6.8 | 0.34 | 0.36 | 0.862! | 1 | 7.361e–15 | – | – | – | 7.361e–15 | C |
| NGC 6528 | 7.9 | 0.54 | 0.13 | 0.266 | 5 | 0.284e–13 | – | – | – | 0.284e–13 | C |
| NGC 6539 | 7.8 | 1.02 | 0.38 | 0.398 | 2 | 0.141e–12 | – | – | – | 0.141e–12 | C |
| NGC 6540 | 5.3 | 0.66 | 0.03 | 0.113! | 1 | 2.059e–14 | 0.078 | 1 | 1.003e–13 | 0.604e–13 | AVE |
| NGC 6544 | 3.0 | 0.76 | 0.05 | 0.087 | 1 | 3.787e–15 | – | – | – | 3.787e–15 | C |
| NGC 6541 | 7.5 | 0.14 | 0.18 | 0.362 | 14 | 0.258e–12 | – | – | – | 0.258e–12 | C |
| 2MS-GC01 | 3.6 | 6.80 | 0.85 | 0.830 | 1 | 5.882e–15 | – | – | – | 5.882e–15 | C |
| ESO-SC06 | 21.4 | 0.07 | 0.60 | – | – | – | – | – | – | – | – |
| NGC 6553 | 6.0 | 0.63 | 0.53 | 0.978 | 14 | 0.952e–13 | 1.004 | 5 | 0.678e–13 | 0.815e–13 | AVE |
| 2MS-GC02 | 4.9 | 5.16 | 0.55 | 0.090 | 1 | 6.753e–14 | – | – | – | 6.753e–14 | C |
| NGC 6558 | 7.4 | 0.44 | 0.03 | 0.401! | 1 | 4.191e–15 | – | – | – | zero flux | C |
| IC 1276 | 5.4 | 1.08 | 1.01 | – | – | – | – | – | – | – | – |
| Terzan 12 | 4.8 | 2.06 | 0.83 | – | – | – | – | – | – | – | – |
| NGC 6569 | 10.9 | 0.53 | 0.35 | 0.650 | 3 | 0.350e–13 | – | – | – | 0.350e–13 | C |
| BH 261 | 6.5 | 0.36 | 0.40 | – | – | – | – | – | – | – | – |
| GLIMPSE 02 | 5.5 | 7.85 | 0.70 | 0.897 | 8 | 0.862e–13 | 0.972 | 8 | 0.223e–12 | 0.155e–12 | AVE |
| NGC 6584 | 13.5 | 0.10 | 0.26 | – | – | – | – | – | – | – | – |
| NGC 6624 | 7.9 | 0.28 | 0.06 | – | – | – | 0.391! | 1 | 1.501e–09 | zero flux | N |
| NGC 6626 | 5.5 | 0.40 | 0.24 | 0.461 | (32) | (0.119e–11) | 0.128 | 1 | 0.172e–09 | 0.172e–09 | N |
| NGC 6638 | 9.4 | 0.41 | 0.22 | 0.264 | 1 | 8.647e–14 | – | – | – | 8.647e–14 | C |
| NGC 6637 | 8.8 | 0.18 | 0.33 | 0.473 | 2 | 0.110e–12 | 0.620 | 3 | 0.160e–12 | 0.135e–12 | AVE |
| NGC 6642 | 8.1 | 0.40 | 0.10 | 0.067 | 1 | 5.310e–15 | – | – | – | 5.310e–15 | C |

**Table 1.** (continued)

| ID | $R_{Sun}$ | E(B–V) | $r_c$ | $r_{max}$ | $n_x$ | $F_X$([0.5−7] keV) Ch./Sw. | $r_{max}$ | $n_x$ | $F_X$([0.5−7] keV) XMMN | Adopted $F_X$([0.5−7] keV) | Mission |
|---|---|---|---|---|---|---|---|---|---|---|---|
| | kpc | mag | arcmin | arcmin | | mW/m$^2$ | arcmin | | mW/m$^2$ | mW/m$^2$ | |
| (1) | (2) | (3) | (4) | (5) | (6) | (7) | (8) | (9) | (10) | (11) | (12) |
| NGC 6652 | 10.0 | 0.09 | 0.10 | 0.134 | 3 | 0.181e–12 | – | – | – | 0.181e–12 | C |
| NGC 6656 | 3.2 | 0.34 | 1.33 | 2.647 | 16 | 0.274e–12 | 2.533 | 9 | 0.244e–12 | 0.259e–12 | AVE |
| Pal 8 | 12.8 | 0.32 | 0.56 | – | – | – | – | – | – | – | – |
| NGC 6681 | 9.0 | 0.07 | 0.03 | 0.013 | 1 | 1.826e–15 | 0.081 | 1 | 0.743e–14 | 0.463e–14 | AVE |
| GLIMPSE 01 | 4.2 | 4.85 | 0.59 | 1.163 | 17 | 0.166e–12 | 0.047 | 1 | 0.456e–12 | 0.311e–12 | AVE |
| NGC 6712 | 6.9 | 0.45 | 0.76 | 1.456 | 8 | 0.147e–09 | – | – | – | 0.147e–09 | C |
| NGC 6715 | 26.5 | 0.15 | 0.09 | 0.178 | 6 | 0.478e–13 | – | – | – | 0.478e–13 | C |
| NGC 6717 | 7.1 | 0.22 | 0.08 | 0.170 | 4 | 0.812e–12 | – | – | – | 0.812e–12 | C |
| NGC 6723 | 8.7 | 0.05 | 0.83 | – | – | – | – | – | – | – | – |
| NGC 6749 | 7.9 | 1.50 | 0.62 | – | – | – | – | – | – | – | – |
| NGC 6752 | 4.0 | 0.04 | 0.17 | 0.173 | 9 | 0.199e–12 | – | – | – | 0.199e–12 | C |
| NGC 6760 | 7.4 | 0.77 | 0.34 | 0.581 | 6 | 0.201e–13 | – | – | – | 0.201e–13 | C |
| NGC 6779 | 9.4 | 0.26 | 0.44 | – | – | – | – | – | – | – | – |
| Terzan 7 | 22.8 | 0.07 | 0.49 | – | – | – | – | – | – | – | – |
| Pal 10 | 5.9 | 1.66 | 0.81 | – | – | – | – | – | – | – | – |
| Arp 2 | 28.6 | 0.10 | 1.19 | – | – | – | – | – | – | – | – |
| NGC 6809 | 5.4 | 0.08 | 1.80 | 3.490 | 21 | 0.145e–12 | 3.498 | 8 | 0.772e–13 | 0.111e–12 | AVE |
| Terzan 8 | 26.3 | 0.12 | 1.00 | – | – | – | – | – | – | – | – |
| Pal 11 | 13.4 | 0.35 | 1.19 | – | – | – | – | – | – | – | – |
| NGC 6838 | 4.0 | 0.25 | 0.63 | 1.262 | 16 | 0.111e–12 | 6.083! | 1 | 6.838e–15 | 0.111e–12 | C |
| NGC 6864 | 20.9 | 0.16 | 0.09 | – | – | – | – | – | – | – | – |
| NGC 6934 | 15.6 | 0.10 | 0.22 | – | – | – | – | – | – | – | – |
| NGC 6981 | 17.0 | 0.05 | 0.46 | – | – | – | – | – | – | – | – |
| NGC 7006 | 41.2 | 0.05 | 0.17 | – | – | – | – | – | – | – | – |
| NGC 7078 | 10.4 | 0.10 | 0.14 | 0.359! | 1 | 4.653e–13 | – | – | – | 4.653e–13 | C |
| NGC 7089 | 11.5 | 0.06 | 0.32 | 0.280 | 3 | 0.304e–13 | 0.100 | 1 | 0.362e–13 | 0.333e–13 | AVE |
| NGC 7099 | 8.1 | 0.03 | 0.06 | 0.125 | 1 | 8.415e–15 | – | – | – | 8.415e–15 | C |
| Pal 12 | 19.0 | 0.02 | 0.02 | – | – | – | – | – | – | – | – |
| Pal 13 | 26.0 | 0.05 | 0.48 | – | – | – | – | – | – | – | – |
| NGC 7492 | 26.3 | 0.00 | 0.86 | – | – | – | 5.514! | 1 | 0.334e–14 | zero flux | N |

## 4 Results and discussion

### 4.1 X-ray luminosity function for globular clusters of the Milky Way

Calculation of the X-ray luminosity $L_X$ (proportional to the total X-ray flux $F_{\rm X}$) of clusters in the Galaxy requires considering not only the distance, but also the absorption of X-ray photons by neutral hydrogen atoms along the line of sight. When X-ray photons pass through a cloud of cool interstellar gas, some of them are absorbed, ionizing the gas.

The equation for radiation transfer in this case has the form:

$$\frac{dF_\nu}{d\nu} = \sigma_\nu n_H F_\nu \,, \tag{1}$$

where the radiation coefficient is equal to zero. In this formula $n_H$ is the concentration of hydrogen atoms and $\sigma_\nu$ is the cross section of photoionization for the K Hydrogen orbit. The cross section of photoionization for the K orbit of the hydrogen-like ions is calculated by the formula:

$$\sigma_\nu = 7.10^{-18} N_K Z^4 \left(\frac{13.56}{h\nu}\right)^3 [\mathrm{cm}^2] \,, \tag{2}$$

where $h\nu$ is the energy of the photon (in eV), $N_K$ is the number of electrons in the K orbit (equal to 1 for hydrogen and hydrogen-like ions, and 2 for other ions), and Z is the charge of atomic nuclei. The transfer equation can be written as:

$$\frac{dF_\nu}{d\tau_\nu} = -F_\nu \,, \tag{3}$$

where $\tau_\nu = \sigma_\nu \int_0^{R_{sun}} N_H \,\mathrm{dr} = \sigma_\nu N_H$, $R_{sun}$ is the globular cluster distance from the Sun, and $N_H$ is the Hydrogen column density along the line of sight measured as the number of atoms in a column with a cross section 1 cm$^2$. The column density of hydrogen $N_H$ is obtained from the color excess E(B–V) of a cluster, given in the catalog of Harris [1996], assuming a standard gas-dust ratio $N_H/\mathrm{E(B-V)} = 4.8 \times 10^{21}$ atoms cm$^{-2}$ mag$^{-1}$ as given in Bohlin et al. [1978]. The real flux can be obtained from the solution of the transfer equation ${F_\nu}^0 = F_\nu \exp(\tau_\nu)$, and then the X-ray luminosity of the cluster is

$$L_X = {F_\nu}^0 4\pi {R_{sun}}^2 \,, \tag{4}$$

for photons with energy 2.3 keV, equal to the effective energy of the X-ray photons, registered by *Chandra* in the range [0.5–7] keV. It should be noted here that even for the clusters with the greatest extinction as GLIMPSE 02,

with color excess E(B–V) = 7.8 mag, X-ray opacity is barely $\tau_\nu = 0.054$, which is due to the weak absorption of solid X-rays by interstellar hydrogen.

Fig. 3 represents the number of GCs vs $\log L_X$, where the function of the X-ray luminosity in the range 0.5 – 7 keV is calculated from the total fluxes of individual sources within $2r_c$ for GCs from the Milky Way. Unfortunately, for 17 of the clusters with a certain X-ray luminosity, the ellipticity is not known, with the largest share in the clusters with high luminosity $\log L_X > 34.5$, where $L_X$ is in units erg s$^{-1}$.

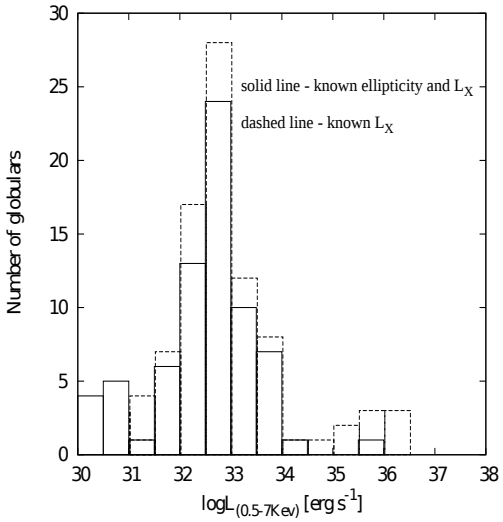


**Fig. 3.** X-ray luminosity function in the range of [0.5–7] keV within 2 core radii for all 89 GCs (solid line) and 72 GCs with known ellipticity (dashed line). Note the lack of that structural parameter for globulars with $\log L_X > 34.5$.

In addition to the ellipticity parameter $\eta$, other data have been extracted from Weatherford et al. [2020] for the estimated number of black holes with an intermediate mass $(\mathrm{N}_{BH}/\mathrm{N}_{cluster}) \times 10^5$, and from Bajkova et al. [2020] for the eccentricity of the orbit $e$ of the GCs. The data for these parameters, together with the calculated luminosities, are given in Table 2, which contains the following columns: the object ID, log $L_X$, ellipticity $\eta$, numbers ratio $\mathrm{N}_{BH}/\mathrm{N}_{cluster}$, eccentricity $e$.

### 4.2 Function K–S tests for samples of X-ray globular clusters of different luminosities

In this research, 52 K–S tests were performed for the ellipticity parameter, varying the limit X-ray luminosity and dividing the clusters into 2 samples: with luminosity greater than or equal to the limit and with a luminosity less than the limit. Data on both ellipticity and X-ray luminosities are available for

**Table 2.** Properties of 89 Milky Way globular clusters used to perform the K–S test

| Globular ID (1) | log $L_X$ [erg $s^{-1}$] (2) | $\eta$ ellipticity (3) | $N_{BH}/N_{cluster}$ $\times 10^5$ (4) | $e$ eccentricity (5) |
|---|---|---|---|---|
| NGC 104 | 33.534 | 0.09 | 2.75 | 0.16 |
| NGC 288 | 32.766 | – | 11.3 | 0.80 |
| NGC 362 | 32.914 | 0.01 | – | 0.98 |
| NGC 1261 | 32.719 | 0.07 | 11.7 | 0.94 |
| Pal 2 | low $L_X$ | 0.05 | – | 0.97 |
| NGC 1851 | 35.801 | 0.05 | 3.22 | 0.99 |
| NGC 1904 | 32.957 | 0.01 | – | 0.97 |
| NGC 2298 | 32.916 | 0.08 | 4.43 | 0.87 |
| NGC 2808 | 36.092 | 0.12 | 5.87 | 0.87 |
| E 3 | 32.131 | – | – | 0.18 |
| NGC 3201 | 32.168 | 0.12 | 13.7 | 0.52 |
| NGC 4372 | 32.810 | 0.15 | – | 0.42 |
| NGC 4590 | 32.775 | 0.05 | 6.81 | 0.54 |
| NGC 5024 | 33.032 | 0.01 | 6.69 | 0.43 |
| NGC 5139 | 33.246 | 0.17 | – | 0.73 |
| NGC 5272 | 33.774 | 0.04 | 3.22 | 0.51 |
| NGC 5286 | 32.734 | 0.12 | 2.53 | 0.89 |
| NGC 5466 | low $L_X$ | 0.11 | 20.3 | 0.80 |
| NGC 5824 | low $L_X$ | 0.03 | – | 0.45 |
| Pal 5 | 33.949 | – | – | 0.27 |
| NGC 5904 | 32.530 | 0.14 | 11.0 | 0.82 |
| NGC 5927 | 32.020 | 0.04 | 17.4 | 0.11 |
| NGC 5946 | 31.656 | 0.16 | – | 0.89 |
| NGC 6093 | 33.234 | 0.00 | 3.03 | 0.97 |
| NGC 6121 | 32.172 | 0.00 | – | 0.97 |
| NGC 6101 | 33.021 | 0.05 | 49.1 | 0.61 |
| NGC 6144 | 32.950 | 0.25 | 14.7 | 0.21 |
| NGC 6139 | 33.035 | 0.05 | – | 0.54 |
| Terzan 3 | 32.318 | – | – | 0.18 |
| NGC 6171 | 32.340 | 0.02 | 13.2 | 0.72 |
| NGC 6205 | 32.920 | 0.11 | 14.1 | 0.79 |
| NGC 6218 | 32.408 | 0.04 | 12.6 | 0.37 |
| NGC 6256 | 33.019 | – | – | 0.92 |
| NGC 6266 | 33.652 | 0.01 | – | 0.62 |
| NGC 6273 | 32.705 | 0.27 | – | 0.59 |
| NGC 6287 | 32.715 | 0.13 | – | 0.75 |
| NGC 6293 | 32.243 | 0.03 | – | 0.91 |
| NGC 6304 | 32.585 | 0.02 | 12.6 | 0.29 |
| NGC 6341 | 32.631 | 0.10 | 3.47 | 0.94 |
| NGC 6325 | 31.815 | 0.12 | – | 0.12 |
| NGC 6333 | 32.011 | 0.04 | – | 0.74 |
| NGC 6342 | 31.149 | 0.18 | – | 0.31 |
| NGC 6355 | 31.824 | – | – | 0.56 |
| Terzan 2 | 35.201 | – | – | 0.86 |
| NGC 6366 | 32.210 | 0.16 | 6.58 | 0.45 |
| Terzan 4 | low $L_X$ | – | – | 0.68 |
| NGC 6362 | 32.514 | 0.07 | – | 0.37 |
| Liller 1 | 35.311 | – | – | 0.81 |
| Terzan 1 | low $L_X$ | – | – | 0.79 |
| NGC 6388 | 33.858 | 0.01 | – | 0.69 |
| NGC 6401 | 32.748 | 0.15 | – | 0.31 |
| NGC 6397 | 32.598 | 0.07 | 1.5 | 0.40 |
| Terzan 5 | 36.251 | – | – | 0.77 |
| NGC 6440 | 34.110 | 0.01 | – | 0.78 |

**Table 2.** (continued)

| Globular ID (1) | log $L_X$ [erg $s^{-1}$] (2) | $\eta$ ellipticity (3) | $N_{BH}/N_{cluster}$ $\times 10^5$ (4) | $e$ eccentricity (5) |
|---|---|---|---|---|
| NGC 6441 | 36.206 | 0.02 | – | 0.66 |
| Terzan 6 | 34.847 | – | – | 0.86 |
| NGC 6453 | 33.393 | 0.09 | – | 0.61 |
| Terzan 9 | 32.761 | – | – | 0.92 |
| Djorg 2 | 33.271 | – | – | 0.57 |
| NGC 6517 | 32.075 | 0.06 | – | 0.90 |
| NGC 6522 | 32.473 | 0.06 | – | 0.67 |
| NGC 6535 | 31.611 | 0.08 | 2.61 | 0.64 |
| NGC 6528 | 32.328 | 0.11 | – | 0.60 |
| NGC 6539 | 33.014 | 0.08 | – | 0.30 |
| NGC 6540 | 32.309 | – | – | 0.32 |
| NGC 6544 | 30.613 | 0.22 | – | 0.98 |
| NGC 6541 | 33.240 | 0.12 | 3.32 | 0.50 |
| NGC 6553 | 32.547 | 0.17 | – | 0.19 |
| NGC 6558 | low $L_X$ | – | – | 0.72 |
| NGC 6569 | 32.698 | 0.00 | – | 0.23 |
| NGC 6624 | low $L_X$ | 0.06 | 0.25 | 0.78 |
| NGC 6626 | 35.795 | 0.16 | – | 0.75 |
| NGC 6638 | 32.962 | 0.01 | – | 0.96 |
| NGC 6637 | 33.098 | 0.01 | 14.6 | 0.94 |
| NGC 6642 | 31.621 | 0.03 | – | 0.94 |
| NGC 6652 | 33.336 | 0.20 | 2.61 | 0.96 |
| NGC 6656 | 32.503 | 0.14 | 6.61 | 0.53 |
| NGC 6681 | 31.652 | 0.01 | 5.94 | 0.74 |
| NGC 6712 | 35.924 | 0.11 | – | 0.94 |
| NGC 6715 | 33.604 | 0.06 | 2.38 | 0.58 |
| NGC 6717 | 33.691 | 0.01 | 2.17 | 0.59 |
| NGC 6752 | 32.581 | 0.04 | 2.09 | 0.23 |
| NGC 6760 | 32.122 | 0.04 | – | 0.44 |
| NGC 6809 | 32.588 | 0.02 | 18.3 | 0.66 |
| NGC 6838 | 32.328 | 0.00 | 17.3 | 0.18 |
| NGC 7078 | 33.780 | 0.05 | 2.55 | 0.50 |
| NGC 7089 | 32.722 | 0.11 | 2.55 | 0.94 |
| NGC 7099 | 31.820 | 0.01 | 1.94 | 0.78 |
| NGC 7492 | low $L_X$ | 0.24 | – | 0.80 |

72 clusters (see Table 2). The test results are presented graphically in Fig. 4, where the confidence level of statistically different ellipticity is obtained by K–S test between a sample with a higher and a sample with a lower than a varying threshold X-ray luminosity $L_{Xlim}$ ([0.5–7] keV). As it can be seen from both representations, the probability of statistical indistinguishability of the ellipticity parameter in X-ray and non-X-ray clusters is lower for higher luminosity limits and varies from 0.2 at $\log L_X^{lim} = 33.65$ to ∼1 at $\log L_X^{lim} = 33.24$. Near the maximum of the X-ray luminosity function $\log L_X^{lim} \sim 32.8$, there is another probability minimum. Therefore, it cannot be postulated that the X-ray and non X-ray clusters in the Galaxy, separated by a luminosity limit $\log L_X^{lim} = 33.65$, are statistically different for significance levels more than 20%. To the extent that the behavior of the probability curve in Fig. 4 is more or less smooth, the accuracy of the measured X-ray luminosities does not affect

the validity of the K–S tests as strongly as the luminosity threshold. Here, it is essential to determine the ellipticity of the clusters with high X-ray luminosity, which is unknown at present. On the other hand, for parameters such as ellipticity, there are no errors are available in the Harris [1996] catalogue. It is assumed to be on the order of one to two hundredths and, therefore, should not severely affect the results of the K–S tests.

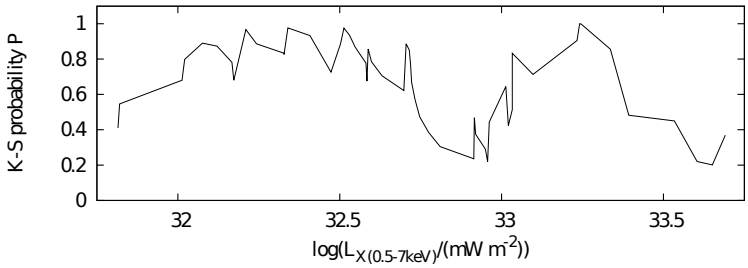


**Fig. 4.** Confidence level of statistically different ellipticity by the means of K–S test between a sample with a higher and a sample with a lower than a varying threshold X-ray luminosity $L_{X\,lim}$ ([0.5–7] keV).

An advantage of the tabular representation (see Table 2) is the possibility to see the mean values and the standard deviation of the ellipticities for both samples. In the present study, the following result was obtained: at limit luminosity $\log L_X^{lim} = 33.65$ clusters with higher X-ray luminosity have an average ellipticity of 0.054, which is 0.03 less than the ellipticity of clusters with X-ray luminosity lower than the limit.

Our knowledge of GCs in the Galaxy has improved recently. Thanks to the data from the Gaia mission, especially for the values of their radial velocities and their proper motions, we now have the spatial velocities and parameters of their orbits such as eccentricity, for instance (Bajkova et al. 2020).

Simioni et al. [2020], analyzing the parametric space of globular clusters, have managed to identify 2 types: some are captured/accreted by the Galaxy, and others are born in it, as the intercepted clusters have orbits that are more eccentric than those of the galactic ones. Sollima [2020] has studied 18 GCs in the Galaxy and, on the basis of increased stellar density, has found tails in 7 of them, which is in turn a fertile field for studying the spatial distribution and kinematics of X-ray sources in them. Accepting threshold value of X-ray luminosity $\log L_X^{lim} = 33.65$ in order to divide the globular clusters from our galaxy into two samples, we conducted 2 more K–S tests for the parameters: estimated number of black holes with intermediate mass $(\mathrm{N}_{BH}/\mathrm{N}_{cluster}) \times 10^5$, according to Weatherford et al. [2020], and the eccentricity of the orbit according to data from Bajkova et al. [2020]. These results, together with the estimation of the ellipticity parameter $\eta$ from Harris [1996], are presented in Fig. 5, which shows the cumulative fractions of GCs vs their ellipticity $\eta$ (upper panel), orbital eccentricity $e$ (middle panel) and number of black holes with intermediate mass $(\mathrm{N}_{BH}/\mathrm{N}_{cluster}) \times 10^5$, repsectively.

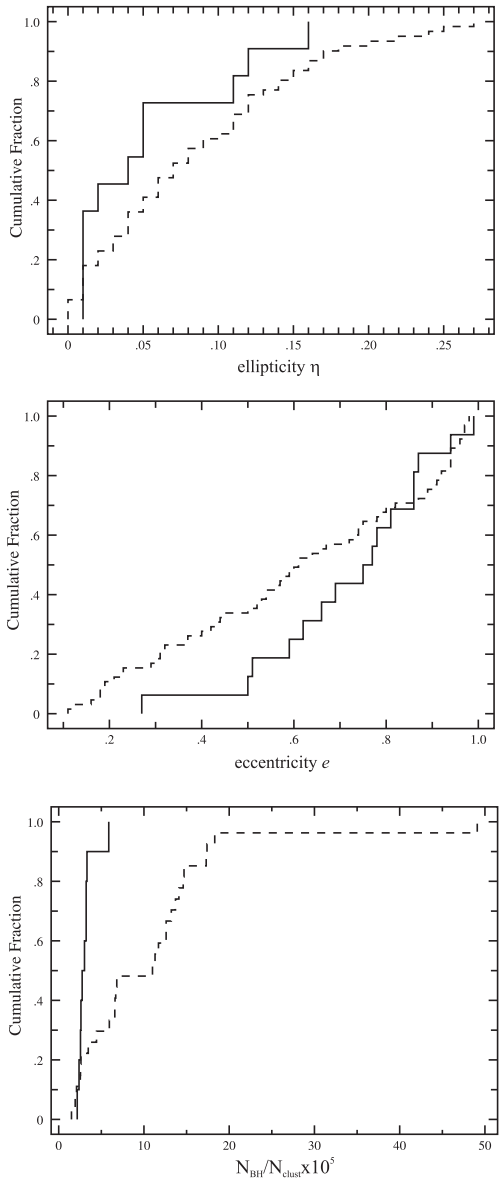


**Fig. 5.** Cumulative probability functions of the globular cluster parameters ellipticity $\eta$ (upper panel), orbital eccentricity $e$ (middle panel) and number of black holes with intermediate mass ($N_{BH}/N_{cluster}$) $\times$ $10^5$ (lower panel) for the samples with X-ray luminosity $L_X > 10^{33.65}$ erg s$^{-1}$ (solid lines) and the samples with X-ray luminosity $L_X \leq 10^{33.65}$ erg s$^{-1}$ (dashed lines).

The hypothesis of statistical indistinguishability can be confidently rejected (for a very high level of significance of 0.999) for the parameter number of black holes with intermediate mass, but the fact that both samples contain only 10 clusters with high and 27 clusters with low X-ray luminosity should be taken into account, and this result should be considered preliminary.

Similar to the results for the ellipticity parameter, for the orbital eccentricity parameter, the statistical indistinguishability hypothesis cannot be rejected with very high confidence (significance level: 0.76).

## Summary and conclusion

On the basis of the results obtained in this research, the following summary and conclusions can be made:

- X-ray fluxes of individual sources detected within 89 Milky Way GCs (Harris,1996) were collected and analised;
- for every cluster in the sample the total X-ray luminosities within $2r_c$ (GC nucleus radius) have been calculated and homogenized and the X-ray luminosity function has been constructed;
- 3 pairs of samples were prepared for three cluster parameters: ellipticity (11 clusters with high and 61 clusters with low X-ray luminosity), eccentricity of the orbit (16 clusters with high and 65 clusters with low X-ray luminosity) and estimated number of black holes with intermediate mass (10 clusters with high and 27 clusters with low X-ray luminosity);
- using the K–S test, the confidence level (expressed in %) of two samples, for which a parameter is available, was estimated to be statistically different. There are indications that the clusters with higher X-ray luminosity are characterized by lower ellipticity, higher eccentricity and a smaller number of black holes with intermediate mass.

### Acknowledgements

This research has made use of the VizieR catalogue access tool, CDS, Strasbourg, France. The Digitized Sky Surveys were produced at the Space Telescope Science Institute under U.S. Government grant NAG W-2166.

This study is financed by the European Union-NextGenerationEU, through the National Recovery and Resilience Plan of the Republic of Bulgaria, project SUMMIT BG-RRP-2.004-0008-C01.

## References

Bajkova, A., et al., 2020, *Milky Way Subsystems from Globular Cluster Kinematics Using Gaia DR2 and HST Data, ApJ, 895, 69*

Barmby, P., et al., 2002, *M31 Globular Clusters in the Hubble Space Telescope Archive. II. Structural Parameters, AJ, 123, 1937*

Barnard, R., et al., 2012, *12 Years of X-Ray Variability in M31 Globular Clusters, Including 8 Black Hole Candidates, as Seen by Chandra, ApJ, 757, 40*

Barnard, R., et al., 2014, *Fifty M31 Black Hole Candidates Identified by Chandra and XMM-Newton, ApJ, 791, 33*

Berg, M., 2019, *X-ray sources in Galactic globular clusters and old open clusters, Proceedings IAU, 14 (S351), 367*

Bohlin, R., et al., 1978, *A survey of interstellar H I from Lalpha absorption measurements, ApJ, 224, 132*
Cheng, Z., et al., 2018, *A Chandra Survey of Milky Way Globular Clusters. I. Emissivity and Abundance of Weak X-Ray Sources, ApJ, 858, 33*
Cheng, Z., et al., 2020, *Exploring the Mass Segregation Effect of X- Ray Sources in Globular Clusters. IV. Evidence of Black Hole Burning in ω Centauri, ApJ, 904, 198*
Di Stefano, R., et al., 2002, *Bright X-ray Sources in M31 Globular Clusters, ApJ, 570, 618*
Evans, I., et al., 2010 – 2019, *The Chandra Source Catalog (CSC), Release 2.0, ApJS, No1, 189, 37*
Evans, P., et al., 2020, *2SXPS An improved and expanded Swift X-ray telescope point source catalogue, ApJS, 247, 54E*
Giesler, M., et al., 2018, *Low-mass X-ray binaries from black hole retaining globular clusters, MNRAS, 477, 1853*
Harris, W.E., 1996, *Catalog of Parameters for Milky Way Globular Clusters, AJ, 112, 1487*
Harris, W.E., 1999, *Globular Cluster Systems, Globular Clusters, CUB (Cambridge University Press)*
King, I., 1981, *The Dynamics of Globular Clusters, QJRAA, 22, 227*
Kong, A., et al., 2002, *X-Ray Point Sources in the Central Region of M31 as Seen by Chandra, ApJ, 577, 738*
Kostov, A., et al., 2005, *Structural Parameters Comparison between X-Ray and Non-X-Ray Globulars in M31, Meetings in Physics at University of Sofia, 6, 86*
Martínez, K., 2019, *Globular Clusters: Jewels to Trace the Structure of Galaxies, PhD thesis, Institute of Astronomy, National Autonomous University of Mexico, Mexico City, Mexico*
Meylan, G., et al., 1997, *Internal dynamics of globular clusters, A&AR, 8, 1, 143*
Ryu, J., et al., 2018, *IDiscovery of Two New Globular Clusters in the Milky Way, ApJ, 863, L38*
Simioni, M., et al., 2020, *Statistical analysis of Galactic globular cluster type properties, MNRAS, 495, 3981*
Sollima, A., 2020, *The eye of Gaia on globular clusters structure: tidal tails, MNRAS, 495, 2222*
Verbunt, F., 2001, *A census with ROSAT of low-luminosity X-ray sources in globular clusters, A&A, 368, 173*
Verbunt, F., et al., 2009, *X-ray Sources in Globular Clusters, ChJAA (Chinese journal of astronomy & astrophysics), 3 (S1), 225*
Weatherford, N., et al., 2020, *A Dynamical Survey of Stellar-mass Black Holes in 50 Milky Way Globular Clusters, ApJ, 898, 162*
Webb, N., et al., 2020, *The XMM-Newton serendipitous survey (IX. The fourth XMM-Newton serendipitous source catalogue), A&A, 641, A136*